JOURNAL OF ENVIRONMENTAL SCIENCES 141 (2024) 225–234

Available online at www.sciencedirect.com

ScienceDirect

www.elsevier.com/locate/jes

JES JOURNAL OF ENVIRONMENTAL SCIENCES

www.jesc.ac.cn

Research Article

Mechanisms of isomerization and hydration reactions of typical β-diketone at the air-droplet interface

Yuemeng Ji[1,2,*], *Weiyong Luo*[1,2], *Qiuju Shi*[1,2], *Xiaohui Ma*[1,2], *Ziqi Wu*[1,2], *Weina Zhang*[1,2], *Yanpeng Gao*[1,2], *Taicheng An*[1,2]

[1] *Guangdong-Hong Kong-Macao Joint Laboratory for Contaminants Exposure and Health, Guangdong Key Laboratory of Environmental Catalysis and Health Risk Control, Institute Environmental Health and Pollution Control, Guangdong University of Technology, Guangzhou 510006, China*

[2] *Guangzhou Key Laboratory of Environmental Catalysis and Pollution Control, Key Laboratory for City Cluster Environmental Safety and Green Development of the Ministry of Education, School of Environmental Science and Engineering, Guangdong University of Technology, Guangzhou 510006, China*

ARTICLE INFO

Article history:
Received 18 February 2023
Revised 13 April 2023
Accepted 13 April 2023
Available online 24 April 2023

Keywords:
Acetylacetone
Air-droplet interface
Theoretical simulation
Isomerization
Hydration reaction mechanism

ABSTRACT

Acetylacetone (AcAc) is a typical class of β-diketones with broad industrial applications due to the property of the keto-enol isomers, but its isomerization and chemical reactions at the air-droplet interface are still unclear. Hence, using combined molecular dynamics and quantum chemistry methods, the heterogeneous chemistry of AcAc at the air-droplet interface was investigated, including the attraction of AcAc isomers by the droplets, the distribution of isomers at the air-droplet interface, and the hydration reactions of isomers at the air-droplet interface. The results reveal that the preferential orientation of two AcAc isomers (*keto*- and *enol*-AcAc) to accumulate and accommodate at the acidic air-droplet interface. The isomerization of two AcAc isomers at the acidic air-droplet interface is more favorable than that at the neutral air-droplet interface because the "water bridge" structure is destroyed by H_3O^+, especially for the isomerization from *keto*-AcAc to *enol*-AcAc. At the acidic air-droplet interface, the carbonyl or hydroxyl O-atoms of two AcAc isomers display an energetical preference to hydration. *Keto*-diol is the dominant products to accumulate at the air-droplet interface, and excessive *keto*-diol can enter the droplet interior to engage in the oligomerization. The photooxidation reaction of AcAc will increase the acidity of the air-droplet interface, which indirectly facilitate the uptake and formation of more *keto*-diol. Our results provide an insight into the heterogeneous chemistry of β-diketones and their influence on the environment.

* Corresponding author.
E-mail: jiym@gdut.edu.cn (Y. Ji).

https://doi.org/10.1016/j.jes.2023.04.013
1001-0742/

Introduction

Oxygenated volatile organic compounds (OVOCs) play an important role in tropospheric chemistry, contributing to the formation of secondary pollutants (ozone and peroxyacetyl nitrate) and secondary organic aerosol (SOA), with implication for air quality, human health, and climate change (Han et al., 2019). The photooxidation of some low-carbon OVOCs can yield extra OVOCs with a larger molecular weight (Zhang et al., 2019), which significantly affect the ability of environmental oxidation (Emmerson et al., 2005; Min et al., 2011; Edwards et al., 2014; Xue et al., 2016). Ketones serve as an important class of OVOCs, with the primary sources involving direct emissions from nature and anthropogenic (such as industrial activities) and secondary production from the environment oxidation of hydrocarbons (Atkinson and Arey, 2003; Romero et al., 2005; Liu et al., 2009; Ji et al., 2018; Brewer et al., 2020). The dominant chemical sink of ketones is photolysis to yield HO_x radicals (such as OH and HO_2) (Arnold et al., 2004; Blitz et al., 2004; Romero et al., 2005) or reaction with the atmospheric oxidants (such as OH and O_3) (Ji et al., 2018; Bedjanian, 2019; Cheramangalath Balan and Rajakumar, 2019; Ji et al., 2020; Chen et al., 2022). Some recent results have shown that most of ketones can enter the aqueous phase or stay at the air-aqueous interface for the oligomerization and photooxidation reactions due to their highly water-soluble, leading to the formation of fine particulate matter (Chen et al., 2008; Kua et al., 2011; Renard et al., 2013; Herrmann et al., 2015; Ji et al., 2020; Mehrani et al., 2021; Ji et al., 2022). β-Diketones are different from conventional aliphatic ketones, since β-diketones simultaneously exist keto-enol isomers due to the isomerization within molecule. Therefore, β-diketones are widely used as organic reagents, catalysts, and chelating ligands in industrial activities, healthcare, perfume, and cosmetics industries due to their structural characteristics (Li et al., 2016). Therefore, some studies paid attention to the form of β-diketones isomers in the environment and the influence factors (Spencer et al., 1982; Folkendt et al., 1985; Ishida et al., 1999; Yamabe et al., 2004; Alagona et al., 2010; Verma et al., 2014; Li et al., 2016). For example, a larger proportion of ketonic isomer in the aqueous phase was found relative to enolic isomer (Spencer et al., 1982) and ketonic isomer is more soluble in polar solvents than the enolic isomer due to a large polarity of ketonic isomer (Ishida et al., 1999). In addition, the chemical oxidation of β-diketonesis complicated and limited by the keto-enol tautomerism (Shouminng et al., 2008; Verma et al., 2014; Kampf et al., 2016; Wu et al., 2016; Ji et al., 2018; Ji et al., 2020), thereby affecting to understand their environment chemical behaviour.

In contrast to the isomerization of β-diketones, limited previous work exists on the aqueous chemistry of β-diketones, hindering accurate assessment of their roles in the environment. In particular, the air-droplet interface chemistry plays a significant role in the field of environmental implications (Pillar-Little et al., 2014; Li et al., 2016; Zhong et al., 2018; Song et al., 2019; Zhang et al., 2019, 2023; Jiang et al., 2020; Ruiz-Lopez et al., 2020; Shi et al., 2020a; Wang et al., 2021; Martins-Costa et al., 2022; Tan et al., 2022a; Gruca-Rokosz et al., 2017). Many chemical reactions rapidly occur at the air-aqueous interface via the different mechanisms relative to the reactions in the aqueous or gas phase, affecting the atmospheric budget of trace gases (Li et al., 2016; Jorgensen and Gross, 2009). In addition, the maximum effective interface area is from 0.3 to 60 m^2/m^3 in environment (George et al., 2015) to attract and adsorb atmospheric trace gases. Hence, the existence of an enough large area suggests that the air-droplet interface chemistry plays a significant role in environment. A recent study has shown that the formation of BrC products is involved by both keto-enol isomers of β-diketones, leading to the resulting complexity of BrC products, and some of these BrC products can give rise to photosensitization reactions to further promote photochemical reactions (Kampf et al., 2016). Therefore, it is necessary to systematically study the isomerization of β-diketones at the air-droplet interface and the subsequent chemical reaction mechanisms.

In this work, we investigated the isomerization and the subsequent hydration mechanisms of typical β-diketones at the air-droplet interface by combining molecular dynamics (MD) simulation and quantum chemical (QC) calculation. Herein, acetylacetone (AcAc) was selected as the model of β-diketones because AcAc was widely detected in environment of developed countries (Japan, America and Europe) and developing countries (China), with its concentration in environment of the parts-per-billion (ppb) level (Ji et al., 2018). The free energy changes with the transformation of the AcAc isomers from the air phase to the droplet interior were calculated and compared at the neutral and acidic air-droplet interfaces. The distribution and proportion of the AcAc isomers in the air phase and droplet interface and interior were assessed. The isomerization and subsequent hydration mechanisms of the *keto*- and *enol*-AcAc at the air-droplet interface were explored, and the implications of the hydration and photooxidation reactions at the air-droplet interface and aqueous-phase hydration reaction on the contribution of environment were discussed.

1. Methods

1.1. Classical molecular dynamics simulations

All classical molecular dynamics (MD) simulations were performed using the NAMD software package (Phillips et al., 2005), and all dynamical configurations were visualized via VMD software (Humphrey et al., 1996). Since the nucleation of the sub-3-nanometer particle is the critical step of aerosol formation (Yao et al., 2018), the neutral and acidic droplet models with $2.5 \times 2.5 \times 2.5$ nm^3 size were constructed. The number of 499 water molecules was used to simulate the neutral droplet because the density of water is 1.0 g/cm^3 and the same water molecules were used in the $24.662 \times 24.662 \times 24.662$ $Å^3$ in the previous studies (Martins-Costa et al., 2012; Shi et al., 2020b). In addition, sulfuric acid solution with 30 wt.% concentration was selected to emulate the acidic droplet, because the atmospheric aerosol exhibits the moderate acidity (Margarella et al., 2013) and the concentration of the sulfuric acid is less than 60 wt.% (Curtius et al., 2001; Zhang et al., 2021). According to the dissociation of sulfuric acid in the experimental study (Margarella et al., 2013), the number of 420

water, 45 hydronium, 23 bisulfate and 11 sulfate ions was determined. The initial positions of the corresponding molecules involved in the neutral and acidic droplets were constructed, respectively, via PACKMOL procedure (Martínez et al., 2009). Subsequently, a 1000 steps optimization and 2.5 ns equilibrium at a time step of 0.5 fs were carried out successively in the isothermal-isochoric (*NVT*) ensemble and isothermal-isobaric (*NPT*) ensemble to ensure the stability of the neutral and acidic droplet models. *N*, *V*, *T* and *P* represent the number of atoms, volume, temperature ($T = 298$ K), and pressure ($P = 1$ bar), respectively. A vacuum layer of 30 Å was added at the equilibrated droplet models along the z-axis direction to simulate the atmospheric process for gaseous acetylacetone (AcAc) approaching into the aqueous phase. In the simulation, the TIP3P, OPLS-AA and CHARMM force fields are determined for water, involved ions and AcAc, respectively. The periodic boundary condition was applied in three dimentions, and a 12 Å cut-off distance was used for Lennard-Jones and real space coulombic interactions. The free-energy profiles of AcAc migrating from the air phase to aqueous phase were obtained by using the umbrella sampling (Torrie and Valleau, 1977; Becke, 1988) and weighted histogram analysis method (WHAM) (Liu et al., 2017). AcAc was initially placed at 2.0 nm above the center of mass (COM) of the neutral and acidic droplets. In the umbrella sampling, 21 windows were set and AcAc moves distance of 1.0 Å each time. The trajectory was carried out for 500 ps at each new position of AcAc. On the other hand, a 50 ns *NVT* simulation for unfixed AcAc at the z-direction was performed to assess the probability distribution of AcAc in the air phase and droplet interface and interior.

1.2. *Born–oppenheimer MD simulations*

To clarify the isomerization and hydration reaction mechanisms of AcAc at the air-droplet interface, the Born-Oppenheimer MD (BOMD) simulations based on the density functional theory (DFT) method were carried out in the CP2K software package (VandeVondele et al., 2005). The exchange and correlation interactions were treated with Becke-Lee-Yang-Parr (BLYP) functional (Lee et al., 1988). The double-ζ Gaussian basis set (DZVP) combined with an auxiliary basis set (VandeVondele and Hutter, 2007) and the Goedecker-Teter-Hutter (GTH) norm-conserved pseudopotentials (Goedecker et al., 1996; Hartwigsen et al., 1998) were used to treat the valence and the core electrons. The Grimme's dispersion correction (DFT-D3) method was adopted to explain the weak dispersion interactions (Grimme, 2004, 2006). A cut-off energy of 280 Rydberg was programmed for the plane wave basis set, and 40 Rydberg was adopted for the Gaussian basis set. The radii of neutral and acidic droplet models were 4.3 Å (Zhong et al., 2017, 2019; Li et al., 2021). In addition, the models with radii of 3.3 and 6.0 Å were also established to prove the selected model's insensitivity to free energy calculation, the details of illustration were presented in Appendix A Fig. S1. The models were placed in cubic boxes greater than 20 Å, which are large enough to eliminate the interaction of adjacent repeat units. Firstly, the droplet models were pre-optimized for 4-5 ps using BOMD simulation to guarantee system stability, and then AcAc molecule was randomly placed above the air-droplet interface. All BOMD simulations were implemented in *NVT* ensemble and the temperature was maintained at 298 K using a Nose-Hoover chain thermostat. The integration step was set to 1.0 fs, which has been proved to achieve good performance for the air-droplet interface reaction (Zhong et al., 2015; Kumar et al., 2017; Tan et al., 2022b). In order to accelerate the some reactions of AcAc at the air-droplet interface, the metadynamics (MTD) simulation was used to calculate the activation free energy (Ensing et al., 2006; Laio and Gervasio, 2008). For each free energy calculation, three sets of parallel metadynamics simulations were conducted to avoid inaccurate results by the instability of the initial configuration. Subsequently, the mean values of the free energies for three sets of simulations were taken to act as the final free energy values discussed. The details of MTD simulation were presented in the Appendix A Supplementary data.

1.3. *Quantum mechanical calculations*

All the geometric optimization and energy calculation for aqueous-phase reactions were performed using Gaussian 09 (Frisch et al., 2013) package suite. The geometric optimization of all stationary points (SPs), including reactants, complex, transition states (TSs), and products, was carried out using the hybrid density functional M06-2X method (Zhao and Truhlar, 2008) with the 6-311G(d,p) basis set (Ji et al., 2017). The method of solvation model based on solute electron density (SMD) (Marenich et al., 2009) was also applied to consider the aqueous effect. The harmonic vibrational frequencies of SPs were calculated to confirm that whether SP is a TS (with only one imaginary frequency) or a minimum (without imaginary frequencies). The intrinsic reaction coordinate (IRC) calculation was performed to confirm that TSs accurately connect with corresponding reactants and products. Based on the above geometries of SPs, single-point energy calculations were further conducted at the M06-2X/6-311+G(3df,3pd) level to refine the energetics and obtain more accurate potential energy surfaces.

2. Results and discussion

2.1. *Gaseous acetylacetone approaching the air-droplet interface*

According to the previous studies (Ji et al., 2018), there is an equilibrium between ketonic and enolic isomers of acetylacetone (denoted as *keto*-AcAc and *enol*-AcAc, respectively). Appendix A Fig. S2 presents the relative concentration distribution profiles of *keto*- and *enol*-AcAc from the air phase to the neutral and acidic droplets. As shown in Appendix A Fig. S2, the relative concentration of neutral and acidic droplets sharply changes from 8.5 to 15.0 Å and 8.0 to 15.0 Å, respectively. Hence, the interfacial width of air and the neutral droplet and that of air and the acidic droplet are estimated to be 6.5 and 7.0 Å, respectively, which can accommodate and adsorb *keto*- and *enol*-AcAc.

The free-energy distribution profiles shown in Appendix A Fig. S3 reveal that the interfaces of the neutral and acidic droplets exhibit the preference to accommodate *keto*- and *enol*-AcAc. To quantify the ability of the interface to adsorb and

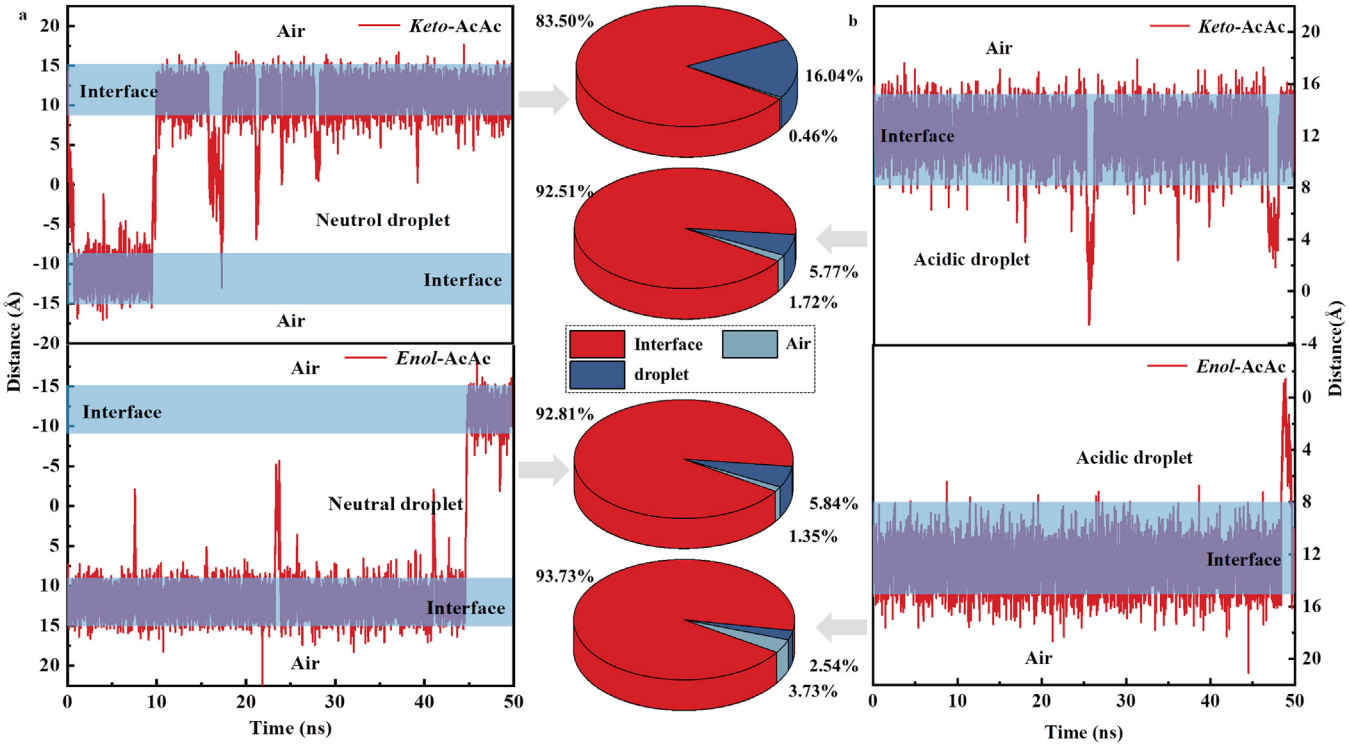

Fig. 1 – Time evolution of the positions of *keto*- and *enol*-AcAc along with the (a) neutral and (b) acidic droplets. The middle data are the corresponding percentages in the air, interface, and interior regions of the droplet.

accommodate two AcAc isomers, the free-energy differences (ΔG) of gaseous AcAc to the interface (air→interface, Process 1) and the interface to the bulk water (interface→aqueous, Process 2) are defined as ΔG(Process1) = $G_{interface}$ - G_{air} and ΔG(Process2) = $G_{aqueous}$ - $G_{interface}$, respectively, where G_{air} represents the maximum values in the air phase (a and a' points in Appendix A Fig. S3), $G_{interface}$ refers to the minimum values at the interface (b and b' points in Appendix A Fig. S3), and $G_{aqueous}$ corresponds to the stable values of *keto*- or *enol*-AcAc in the interior region of droplet (c and c' points in Appendix A Fig. S3). The ΔG value reflects the above two processes are endothermic or exothermic (Shi et al., 2020a). For the acidic droplet, the $\Delta G_{air\rightarrow interface}$ values of *keto*- and *enol*-AcAc are -7.49 and -5.99 kcal/mol, respectively, which are more negative than the corresponding values in the neutral droplet. Also, their $\Delta G_{interface\rightarrow aqueous}$ values of 3.70 and 3.08 kcal/mol, respectively, are larger than those in the neutral droplet. It indicates that AcAc prefers to be adsorbed to the acidic air-droplet interface if AcAc molecules collide with the droplets.

Fig. 1 shows the time evolution of the positions (z coordinate) of *keto*- and *enol*-AcAc in the neutral and acidic droplets in every residence event. The probabilities of *keto*- and *enol*-AcAc staying at the acidic air-droplet interface are presented at 92.51% and 93.73% of the whole simulated time (Fig. 1a), respectively, in line with the analysis of the free energy calculations mentioned above. The duration time of *keto*-AcAc in the interior region of acidic air-droplet interface accounts for 5.77% of the whole simulated time, which is two times larger than that of *enol*-AcAc (Fig. 1a), attributable to the stronger polarity of *keto*-AcAc than *enol*-AcAc in the bulk water (Ishida et al., 1999). That is, for β-diketones, the ketonic and enolic isomers are prone to accumulate at the air-droplet interface, especially at the acidic air-droplet interface; while relative to the enolic isomer, the ketonic isomer prefers to stay in the interior region of the droplet.

2.2. *Isomerization between* keto- *and* enol-AcAc

The isomerization of β-diketones can affect the interpretation of chemical mechanisms occurring on the nanoparticle interfaces. Therefore, to clarify the distribution of *keto*- and *enol*-AcAc at the air-droplet interfaces, we investigated the isomerization reactions between *keto*- and *enol*-AcAc at the neutral and acidic air-droplet interface. Fig. 2 shows the free-energy landscape and the schematic diagram of the corresponding structures for the isomerization from *keto*-AcAc to *enol*-AcAc. Appendix A Fig. S4 displays the time variation of bond lengths between relevant atoms of the isomerization. Appendix A Fig. S4 suggests that the small water clusters are formed around AcAc to mediate the isomerization. There are three-step reactions in the isomerization from *keto*-AcAc to *enol*-AcAc (Appendix A Fig. S4a): the first H-shift from *keto*-AcAc to water molecule (R1), the second H-shift in the water cluster (R2), and the *enol*-AcAc formation from the third H-shift (R3).

For R1 (along blue dashed arrow), the methylene H atom (H_K1) of *keto*-AcAc is transferred to the first water molecule (W1) to form a H-bond (H_K1-O_{W1}) at 6.12 ps, with the H_K1-O_{W1} distance of 2.00 Å. Subsequently, a maximum of free energy (27.00 kcal/mol) is observed at 7.02 ps, corresponding to form the H_K1-O_{W1} bond and break the C_K1-H_K1 bond in *keto*-AcAc,

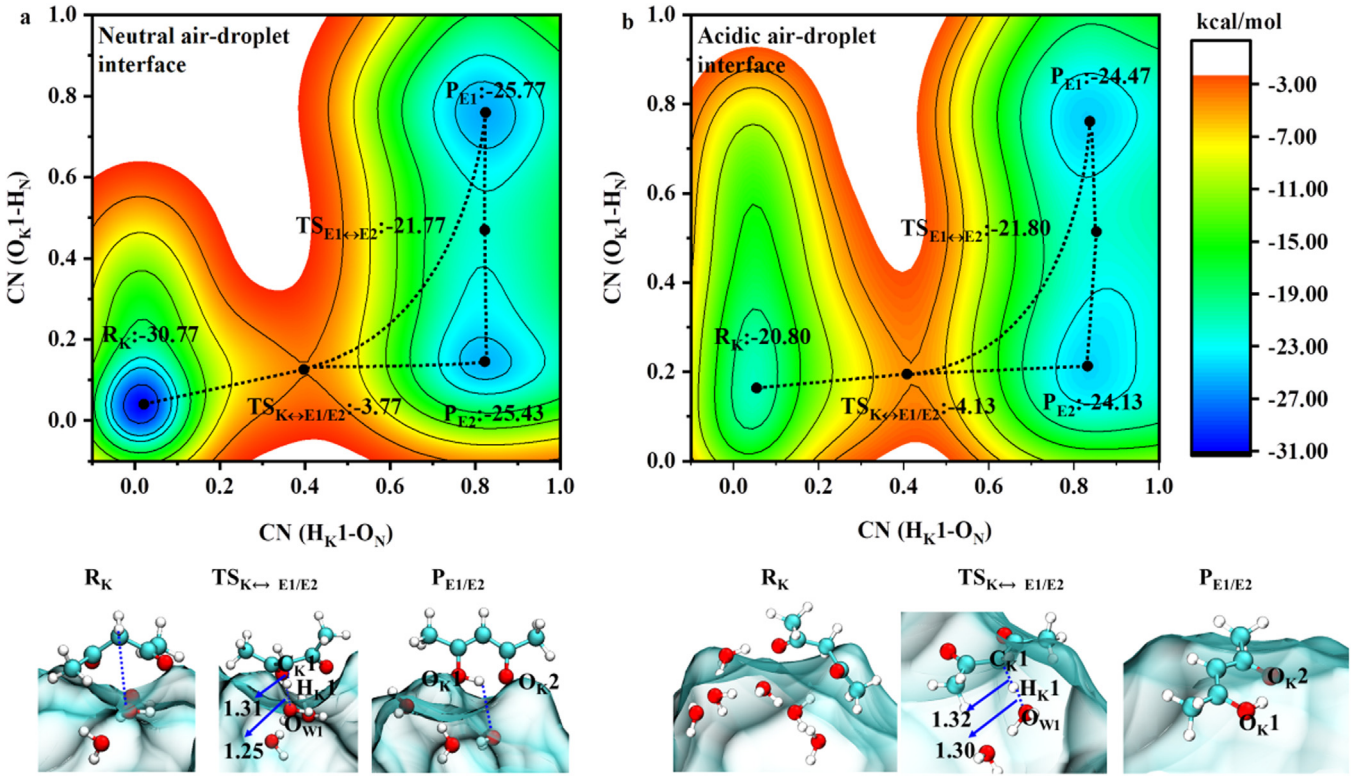

Fig. 2 – Free energy landscapes and the schematic diagrams of the corresponding structures in the isomerization of *keto*-AcAc to *enol*-AcAc at the (a) neutral and (b) acidic air-droplet interfaces. R, TS and P represent reactants, transition states and products, respectively.

suggesting the transition state formation. The lengths of the H_K1-O_{W1} and C_K1-H_K1 bonds in the transition-state are 1.25 and 1.31 Å, respectively (Fig. 2a). As for R2 (from 7.03 to 7.21 ps, along green dashed arrow), an extra H-shift reaction proceeds via the second water (W2) to the third water (W3) to yield hydronium ion (H_3O^+). For R3 (along yellow dashed arrow), the shift of $H_{W3}1$ atom to the carbonyl O atom of *keto*-AcAc (O_K1/2) yields *enol*-AcAc, and the system reaches equilibrium at 7.22 ps. As shown in Fig. 2a, two local minimums of the free energies are observed because the H atom is moved between carbonyl and hydroxyl O atoms, corresponding to one *enol*-AcAc formation. It implies that *enol*-AcAc has a conjugated π-electron character and enhances the stability of *enol*-AcAc. As discussed above, R2 acts as a "bridge" between R1 and R3, suggesting that the presence of a water-loop-structure has a catalytic effect on the isomerization from *keto*-AcAc to *enol*-AcAc.

However, no water-loop-structure event at the acidic air-droplet interface is observed in the isomerization because of two water clusters around AcAc. As shown in Appendix A Fig. S4b, one two-water cluster engages in the first H-shift to form *keto*-anion (R1, in blue dashed arrow), and one three-water cluster simultaneously participates in the second H-shift to yield H_3O^+ (R2, in green dashed arrow). The H_3O^+ formed in R2 is transferred to *keto*-anion in R1 to form *enol*-AcAc (R3, yellow dashed arrow). A transition state-like structure is observed at 8.96 ps, with the corresponding free-energy barrier of 16.67 kcal/mol (Fig. 2b), which is 10.33 kcal/mol lower than that at the neutral air-droplet interface. It is explained by the proton affinity (ΔPA) of H_2O according to that ΔPA increases with increasing the numbers of water molecules (n), since at n more than 3, the ΔPA of $H_2O + H_3O^+$ reaction is larger than that of *enol*-AcAc + H_3O^+ reaction (Mauney et al., 2017). Combined with the analysis of Section 2.1, it implies that *enol*-AcAc is enhanced in favor of the enolic isomer at the acidic air-droplet interface relative to the neutral air-droplet interface.

2.3. *Hydration reactions of AcAc at the air-droplet interface*

Considering the results mentioned above and the acidity in real aerosols, we focus on investigating the hydration reaction of *enol*-AcAc at the acidic air-droplet interface, since the hydration reaction is considered to be the first step of the oligomerization for OVOCs (Mauney et al., 2017), leading to oligomeric products which contribute to SOA growth. For comparison, the hydration reaction of *keto*-AcAc is also studied. Fig. 3 shows a schematic diagram of three stepwise pathways of the hydration reactions for *enol*-AcAc. Appendix A Figs. S5-S6 display the free-energy distribution diagram of the hydration reactions of *enol*-AcAc. Fig. 4 displays the change curves of key distances, the two-dimensional free-energy distribution diagram, and the geometry diagrams of the key stability points in the hydration reactions of *keto*-AcAc.

The interfacial hydration of *enol*-AcAc involves four-step reactions: (I) H-shift process (blue line), (II) cation-intermediate formation (green line), (III) transition-state for-

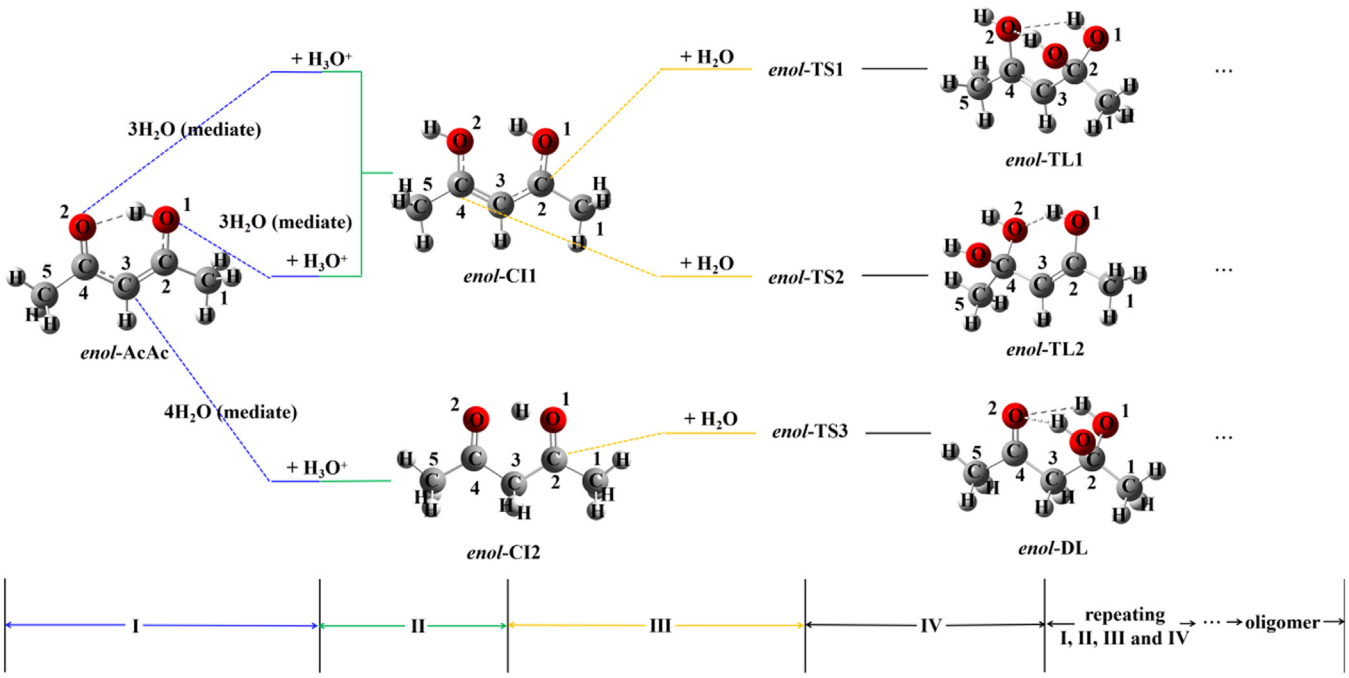

Fig. 3 – A schematic diagram of three stepwise pathways of the hydration reactions for *enol*-AcAc at the acidic air-droplet interface.

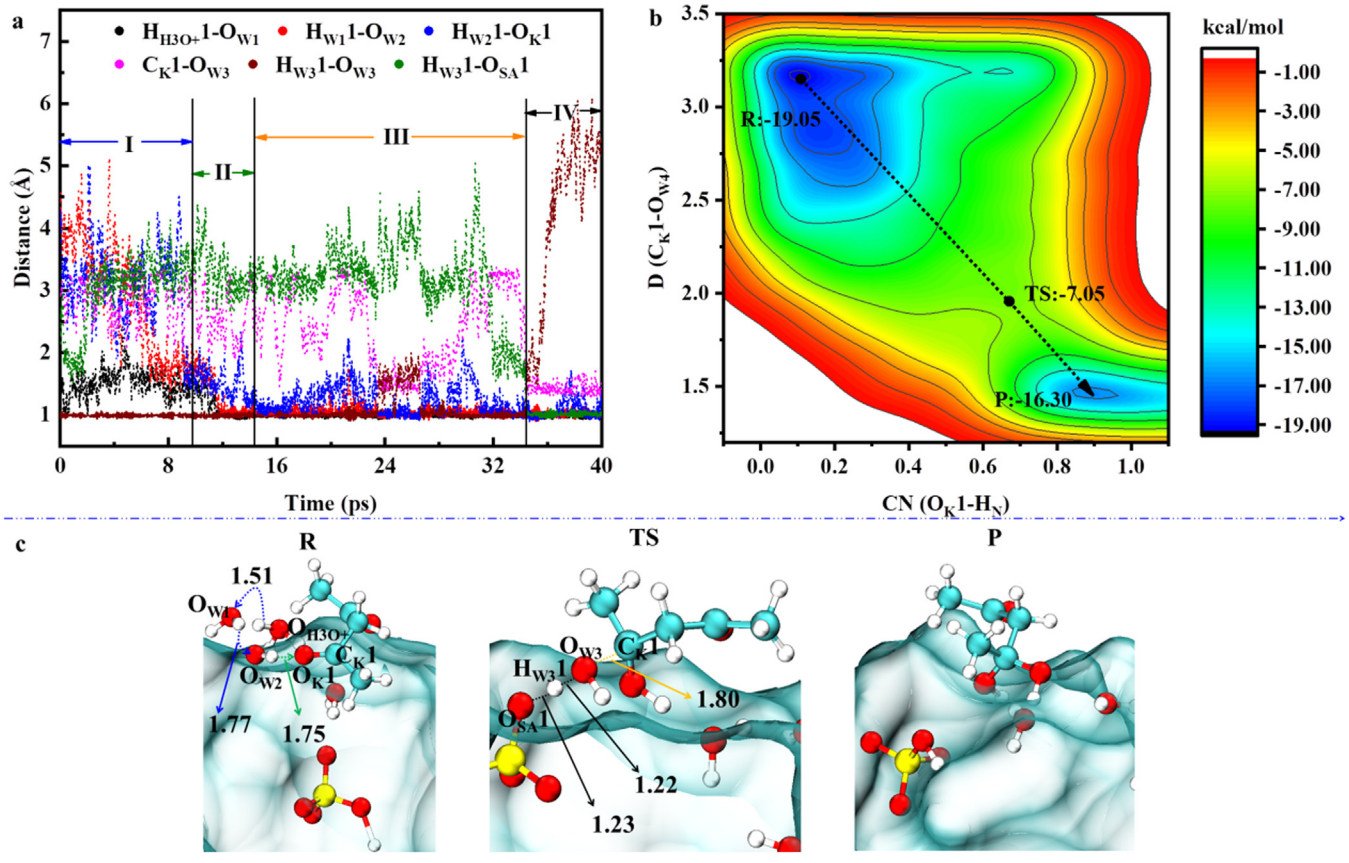

Fig. 4 – (a) Change curves of key distances, (b) two-dimensional free energy distribution diagram, and (c) geometry diagrams of key stability points in the hydration reactions of *keto*-AcAc at the acidic air-droplet interface. R, TS and P represent the reactant, transition state and product, respectively, and the unit of bond length is Å.

mation (yellow line), (IV) diol formation (black line), and details of the multi-step hydration reactions are illustrated in Fig. 3. For the first step, the H-shift can be occurred at three reactive sites of *enol*-AcAc, hydroxyl (O_E1) and carbonyl (O_E2) O-atoms and double-bond C-atom (C_E3). Therefore, the O_E1-H_W3, O_E2-H_W3, and C_E3-H_W4 bonds are formed via the H-shift processes from hydronium ion to water molecules to three reactive sites of *enol*-AcAc, with the corresponding lengths of 2.08, 2.01, and 1.50 Å, respectively. Subsequently, the O_E1-H_W3, O_E2-H_W3, and C_E3-H_W4 bonds are shorten to 1.02, 1.02, and 1.07 Å, respectively, to form two *enol*-cation intermediates (*enol*-CI1 and *enol*-CI2). For the step III, a transition-state-like structure for the reaction starting with the double-bond (*enol*-TS3) is observed, corresponding to the free-energy maximum with 43.67 kcal/mol (Appendix A Fig. S5), which is larger than those starting with hydroxyl/carbonyl group (*enol*-TS1 and *enol*-TS2) (Appendix A Fig. S6). It suggests that the hydroxyl/carbonyl O-atoms are the most energetically favorable position to proceed via hydration for *enol*-AcAc, to form the *enol*-triols (*enol*-TLs).

Similarly, the hydration of *keto*-AcAc also contains the same four-step reactions (Fig. 4a). However, the H-shift process of *keto*-AcAc starts with carbonyl O atom group based on the structural characteristics of *keto*-AcAc. Through two H-shift processes from hydronium ion to water molecules (W1 and W2), the O_K1-$H_{W2}1$ bond is formed at 9.36 ps, with the length of 2.02 Å. During a period from 14.60 to 34.40 ps (III), the maximum of free energy (12.00 kcal/mol) is observed at 34.37 ps (Fig. 4b), corresponding to a transition-state-like structure (Fig. 4c), which is 7.33 kcal/mol lower than that of the dominate hydration pathway for *enol*-AcAc starting with hydroxyl/carbonyl group, suggesting the more favorable formation of *keto*-diol (*keto*-DL) than *enol*-TL1 and *enol*-TL2. Combined with the above analysis about the isomerization reaction of AcAc, it indicates that *enol*-AcAc accumulated at the interface is preferentially converted to form *keto*-AcAc, and *keto*-DL is subsequently yielded by the proton-mediated hydration reaction of *keto*-AcAc.

Subsequently, *keto*-DL proceeds the hydration reaction via the similar four-step reactions (Appendix A Fig. S7a): (I) H-shift process ($t < 15.91$ ps); (II) cation-intermediate formation ($15.91 \leq t < 16.06$ ps); (III) transition-state formation ($16.06 \leq t < 22.36$ ps); (IV) tetrol formation ($t \geq 22.36$ ps). As illustrated in the SI, the process of *keto*-DL to form *keto*-tetrol via the proton-mediated hydration reaction is endothermic with a large free-energy barrier of 16.67 kcal/mol (Appendix A Fig. S7b). It indicates that the proton-mediated hydration reaction of *keto*-DL is an energetically unfavorable pathway, leading to the accumulation and accommodation of *keto*-DL at the acidic air-droplet interface.

3. Conclusions and atmospheric implications

β-Diketones are a special class of ketones, which are widely used as organic reagents, catalysts, and chelating ligands in industrial activities, healthcare, perfume, and cosmetics industries due to the property of the simultaneous presence of keto-enol isomers. Acetylacetone (AcAc) is a typical kind of β-diketones, but its isomerization and chemical behavior at the air-droplet interface are still unclear, leading to affect to assess its environmental effects. Hence, we investigated the heterogeneous chemistry of AcAc at the neutral and acidic air-droplet interfaces by combining molecular dynamics (MD) and quantum chemistry (QC), and the influence of interfacial acidity on the chemical behavior of AcAc was also evaluated. Our MD simulation results reveal that two AcAc isomers, *enol*-AcAc and *keto*-AcAc, are prone to be adsorbed by the neutral and acidic air-droplet interfaces, but the acidic air-droplet interface exhibits a better ability to accumulate and accommodate two AcAc isomers, especially for *enol*-AcAc. The isomerization of two AcAc isomers at the air-droplet interface all involves three-step reactions, the H-shift of AcAc to the interfacial water, the H-shift between the water clusters, and the formation of other AcAc isomer. At the neutral air-droplet interface, the isomerization of AcAc isomer undergoes a "water bridge" mechanism, while the "water bridge" structure is destroyed by much H_3O^+ at the acidic air-droplet interface. Therefore, the isomerization from *keto*-AcAc to *enol*-AcAc is more favorable than that from *enol*-AcAc to *keto*-AcAc, and the enolic isomer is the dominant form of the accommodation for AcAc at the acidic air-droplet interface.

Subsequently, *enol*-AcAc undergoes the H-shift via water molecules to form low-volatile compounds at the acidic air-droplet interface. Hydration at the carbonyl or hydroxyl O-atom of *enol*-AcAc is the most energetically favorable pathway, forming the *enol*-triols (*enol*-TLs). However, its free-energy barrier is larger than that of the isomerization from *enol*-AcAc to *keto*-AcAc. Alternatively, the hydration of *keto*-AcAc starting with the carbonyl O-atom mainly produces *keto*-DL, with a low free-energy barrier. Hence, the main product of the hydration reaction of AcAc at the acidic air-droplet interface is *keto*-DL, whose proton-mediated hydration reaction is an energetically unfavorable pathway, leading to the accumulation and accommodation of *keto*-DL at the acidic air-droplet interface.

To assess the contribution of the interface chemical behavior of AcAc to the whole aqueous chemistry, the hydration reaction of *keto*-DL in bulk water is further investigated, to simulate the main interface product entering the acidic droplet interior (Appendix A Fig. S8). There exists two-steps hydration reaction of *keto*-DL: protonation and nucleophilic addition. As shown in Appendix A Fig. S8, protonation at the carbonyl O-atom site of *keto*-DL is slightly exergonic to form cationic intermediate, with the reaction energy value of -2.87 kcal/mol. Nucleophilic addition between cationic intermediate and water molecules possesses a TS with the activation barrier of 10.69 kcal/mol, which is 5.98 kcal/mol lower than that at the air-droplet interface (Appendix A Fig. S7b). It indicates that excessive *keto*-DL can enter the droplet interior to engage in the oligomerization, thereby facilitating the air-droplet interface to accommodate and yield more *keto*-DL.

On the other hand, to systematically understand the interface chemistry of AcAc, the oxidation reaction of *keto*-DL with OH radical (·OH) at the acidic air-droplet interface is also evaluated to simulate the photooxidation (Appendix A Fig. S9). H-abstraction from the methyl or methylene group of *keto*-DL forming *keto*-DL radical is barrierless. However, H-abstraction from the hydroxyl group of *keto*-DL is barrierless, accompanied by the breakage of C_b-C_c bond to rapidly form acetic acid (AA). The breakage of C_b-C_c bond needs to overcome the activation

barrier of 8.47 kcal/mol (Appendix A Fig. S9a and b). Alternatively, an adduct is yielded by OH-addition to the carbonyl C-atom of *keto*-DL, with the free-energy barrier of 9.40 kcal/mol. Subsequently, the C_c-C_d bond in the adduct is broken to yield AA, with the activation barrier of 4.04 kcal/mol (Appendix A Fig. S9a and c). It suggests that the photooxidation reaction of AcAc will increase the acidity of the air-droplet interface, further promoting the accommodation and the proton-mediated hydration reaction of AcAc. Our work reveals that we should focus on not only the isomerization and chemical reactions of the β-diketones (such as AcAc) at the air-droplet interface, but also their photooxidation reactions in the future studies. Our results provide an insight into the heterogeneous reaction mechanisms of β-diketones and their influence on the environment.

Declaration of Competing Interest

The authors declare that they have no known competing financial interests or personal relationships that could have appeared to influence the work reported in this paper.

Acknowledgments

This work was supported by the Guangdong Basic and Applied Basic Research Foundation (No. 2019B151502064), the National Natural Science Foundation of China (Nos. 42077189, 42020104001, and 42277081), the Local Innovative and Research Teams Project of Guangdong Pearl River Talents Program (No. 2017BT01Z032), the Science and Technology Key Project of Guangdong Province, China (No. 2019B110206002), and the Guangdong Provincial Key R&D Program (No. 2022-GDUT-A0007).

Appendix A Supplementary data

Supplementary material associated with this article can be found in the online version at doi:10.1016/j.jes.2023.04.013.

References

Alagona, G., Ghio, C., Nagy, P.I., 2010. The catalytic effect of water on the keto-enol tautomerism. Pyruvate and acetylacetone: a computational challenge. Phys. Chem. Chem. Phys. 12, 10173.

Arnold, S.R., Chipperfield, M.P., Blitz, M.A., Heard, D.E., Pilling, M.J., 2004. Photodissociation of acetone: atmospheric implications of temperature-dependent quantum yields. Geophys. Res. Lett. 31, 1–4.

Atkinson, R., Arey, J., 2003. Atmospheric degradation of volatile organic compounds. Chem. Rev. 103, 4605–4638.

Becke, A.D., 1988. Density-functional exchange-energy approximation with correct asymptotic behavior. Phys. Rev. A 38, 3098–3100.

Bedjanian, Y., 2019. Temperature-dependent rate constant for the reaction of hydroxyl radical with 3-hydroxy-3-methyl-2-butanone. J. Phys. Chem. A 123, 10446–10453.

Blitz, M.A., Heard, D.E., Pilling, M.J., Arnold, S.R., Chipperfield, M.P., 2004. Pressure and temperature-dependent quantum yields for the photodissociation of acetone between 279 and 327.5 nm. Geophys. Res. Lett. 31, L06111.

Brewer, J.F., Fischer, E.V., Commane, R., Wofsy, S.C., Daube, B.C., Apel, E.C., et al., 2020. Evidence for an oceanic source of methyl ethyl ketone to the atmosphere. Geophys. Res. Lett. 47 e2019GL086045.

Chen, L., Huang, Y., Xue, Y., Jia, Z., Wang, W., 2022. Kinetic and mechanistic investigations of OH-Initiated atmospheric degradation of methyl butyl ketone. J. Phys. Chem. A 126, 2976–2988.

Chen, Z.M., Wang, H.L., Zhu, L.H., Wang, C.X., Jie, C.Y., Hua, W., 2008. Aqueous-phase ozonolysis of methacrolein and methyl vinyl ketone: a potentially important source of atmospheric aqueous oxidants. Atmos. Chem. Phys. 8, 2255–2265.

Cheramangalath Balan, R., Rajakumar, B., 2019. Photo-oxidation reaction kinetics and mechanistics of 4-hydroxy-2-butanone with Cl atoms and OH radicals in the gas phase. J. Phys. Chem. A 123, 4342–4353.

Curtius, J., Sierau, B., Arnold, F., de Reus, M., Ström, J., Scheeren, H.A., et al., 2001. Measurement of aerosol ulfuric acid: 2. Pronounced layering in the free troposphere during the second aerosol characterization experiment (ACE 2). J. Geophys. Res. 106, 31975–31990.

Edwards, P.M., Brown, S.S., Roberts, J.M., Ahmadov, R., Banta, R.M., DeGouw, J.A., et al., 2014. High winter ozone pollution from carbonyl photolysis in an oil and gas basin. Nature 514, 351–354 (London).

Emmerson, K.M., Carslaw, N., Pilling, M.J., 2005. Urban atmospheric chemistry during the PUMA campaign 2: radical budgets for OH, HO_2 and RO_2. J. Atmos. Chem. 52, 165–183.

Ensing, B., De Vivo, M., Liu, Z., Moore, P., Klein, M.L., 2006. Metadynamics as a tool for exploring free energy landscapes of chemical reactions. Acc. Chem. Res. 39, 73–81.

Folkendt, M.M., Weiss-Lopez, B.E., Chauvel, J.P., True, N.S., 1985. Gas-Phase 1H NMR studies of Keto-Enol tautomerlsm of acetylacetone, methyl acetoacetate, and ethyl acetoacetate. J. Phys. Chem. 89, 3347–3352.

Frisch, M.J., Trucks, G.W., Schlegel, H.B., Scuseria, G.E., Robb, M.A., Cheeseman, J.R., et al., 2013. Gaussian 09, Revision D.01, Gaussian, Inc., Wallingford CT.

George, C., Ammann, M., D Anna, B., Donaldson, D.J., Nizkorodov, S.A., 2015. Heterogeneous photochemistry in the atmosphere. Chem. Rev. 115, 4218–4258.

Goedecker, S., Teter, M., Hutter, J., 1996. Separable dual-space Gaussian pseudopotentials. Phys. Rev. B Condensed Matter 54, 1703–1710.

Grimme, S., 2004. Accurate description of van der Waals complexes by density functional theory including empirical corrections. J. Comput. Chem. 25, 1463–1473.

Grimme, S., 2006. Semiempirical GGA-type density functional constructed with a long-range dispersion correction. J. Comput. Chem. 27, 1787–1799.

Gruca-Rokosz, R., Bartoszek, L., Koszelnik, P., 2017. The influence of environmental factors on the carbon dioxide flux across the water-air interface of reservoirs in south-eastern Poland. J. Environ. Sci. 56, 290–299.

Han, Y., Huang, X., Wang, C., Zhu, B., He, L., 2019. Characterizing oxygenated volatile organic compounds and their sources in rural atmospheres in China. J. Environ. Sci. 81, 148–155.

Hartwigsen, C., Goedecker, S., Hutter, J., 1998. Relativistic separable dual-space Gaussian Pseudopotentials from H to Rn. Phys. Rev. B 58, 3641–3662.

Herrmann, H., Schaefer, T., Tilgner, A., Styler, S.A., Weller, C., Teich, M., et al., 2015. Tropospheric aqueous-phase chemistry: kinetics, mechanisms, and its coupling to a changing gas phase. Chem. Rev. 115, 4259–4334.

Humphrey, W., Dalke, A., Schulten, K., 1996. VMD: visual molecular dynamics. J. Mol. Graph. 14 (33-38), 27–28.
Ishida, T., Hirata, F., Kato, S., 1999. Thermodynamic analysis of the solvent effect on tautomerization of acetylacetone: anab initio approach. J. Chem. Phys. 110, 3938–3945.
Ji, Y., Qin, D., Zheng, J., Shi, Q., Wang, J., Lin, Q., et al., 2020. Mechanism of the atmospheric chemical transformation of acetylacetone and its implications in night-time second organic aerosol formation. Sci. Total Environ. 720, 137610.
Ji, Y., Shi, Q., Ma, X., Gao, L., Wang, J., Li, Y., et al., 2022. Elucidating the critical oligomeric steps in secondary organic aerosol and brown carbon formation. Atmos. Chem. Phys. 22, 7259–7271.
Ji, Y., Zhao, J., Terazono, H., Misawa, K., Levitt, N.P., Li, Y., Lin, Y., et al., 2017. Reassessing the atmospheric oxidation mechanism of toluene. Proc. Natl. Acad. Sci. 114, 8169–8174.
Ji, Y., Zheng, J., Qin, D., Li, Y., Gao, Y., Yao, M., et al., 2018. OH-Initiated oxidation of acetylacetone: Implications for ozone and secondary organic aerosol formation. Environ. Sci. Technol. 52, 11169–11177.
Jiang, X.T., Lv, C., You, B., Liu, Z.Y., Wang, X.F., Du, L., 2020. Joint impact of atmospheric SO_2 and NH_3 on the formation of nanoparticles from photo-oxidation of a typical biomass burning compound. Environ. Sci. Nano 7, 2532–2545.
Jorgensen, S., Gross, A., 2009. Theoretical investigation of the reaction between carbonyl oxides and ammonia. J. Phys. Chem. A 113, 10284–10290.
Kampf, C.J., Filippi, A., Zuth, C., Hoffmann, T., Opatz, T., 2016. Secondary brown carbon formation via the dicarbonyl imine pathway: nitrogen heterocycle formation and synergistic effects. Phys. Chem.Chem. Phys. 18, 18353–18364.
Kua, J., Krizner, H.E., De Haan, D.O., 2011. Thermodynamics and kinetics of imidazole formation from glyoxal, methylamine, and formaldehyde: A computational study. J. Phys. Chem. A 115, 1667–1675.
Kumar, M., Zhong, J., Francisco, J.S., Zeng, X.C., 2017. Criegee intermediate-hydrogen sulfide chemistry at the air/water interface. Chem. Sci. 8, 5385–5391.
Laio, A., Gervasio, F.L., 2008. Metadynamics: a method to simulate rare events and reconstruct the free energy in biophysics, chemistry and material science. Rep. Prog. Phys. 71, 126601.
Lee, C., Yang, W., Parr, R.G., 1988. Development of the Colle-Salvetti correlation-energy formula into a functional of the electron density. Phys. Rev. B Condens Matter 37, 785–789.
Li, L., Kumar, M., Zhu, C., Zhong, J., Francisco, J.S., Zeng, X.C., 2016. Near-barrierless ammonium bisulfate formation via a loop-structure promoted proton-transfer mechanism on the surface of water. J. Am. Chem. Soc. 138, 1816–1819.
Li, H., Wang, X., Zhong, J., Chu, B., Ma, Q., Zeng, X., 2021. Mechanistic study of the aqueous reaction of organic peroxides with HSO_3^- on the Surface of a water droplet. Angew. Chem. Int. Ed. 60, 20200–20203.
Liu, M., Song, Y., Zhou, T., Xu, Z., Yan, C., Zheng, M., et al., 2017. Fine particle pH during severe haze episodes in northern China. Geophys. Res. Lett. 44, 5213–5221.
Liu, Y., Shao, M., Kuster, W.C., Goldan, P.D., Li, X., Lu, S., et al., 2009. Source identification of reactive hydrocarbons and oxygenated VOCs in the summertime in Beijing. Environ. Sci. Technol. 43, 75–81.
Marenich, A.V., Cramer, C.J., Truhlar, D.G., 2009. Universal solvation model based on solute electron density and on a continuum model of the solvent defined by the bulk dielectric constant and atomic surface tensions. J. Phys. Chem. B 113, 6378–6396.
Margarella, A.M., Perrine, K.A., Lewis, T., Faubel, M., Winter, B., Hemminger, J.C., 2013. Dissociation of sulfuric acid in aqueous solution: Determination of the photoelectron spectral fingerprints of H_2SO_4, HSO_4^-, and SO_4^{2-} in water. J. Phys. Chem. C 117, 8131–8137.
Martínez, L., Andrade, R., Birgin, E.G., Martínez, J.M., 2009. PACKMOL: a package for building initial configurations for molecular dynamics simulations. J. Comput. Chem. 30, 2157–2164.
Martins-Costa, M.T.C., Anglada, J.M., Francisco, J.S., Ruiz-Lopez, M.F., 2012. Reactivity of volatile organic compounds at the surface of a water droplet. J. Am. Chem. Soc. 134, 11821–11827.
Martins-Costa, M.T.C., Anglada, J.M., Francisco, J.S., Ruiz-López, M.F., 2022. Photosensitization mechanisms at the air-water interface of aqueous aerosols. Chem. Sci. 13, 2624–2631.
Mauney, D.T., Maner, J.A., Duncan, M.A., 2017. IR spectroscopy of protonated acetylacetone and its water clusters: enol-keto tautomers and ion→ solvent proton transfer. J. Phys. Chem. A 121, 7059–7069.
Mehrani, S., Tayyari, S.F., Heravi, M.M., Morsali, A., 2021. Theoretical investigation of solvent effect on the keto-enol tautomerization of pentane-2,4-dione and a comparison between experimental data and theoretical calculations. Can. J. Chem. 99, 411–424.
Min, S., Bin, W., Sihua, L., Bin, Y., Ming, W., 2011. Effects of Beijing olympics control measures on reducing reactive hydrocarbon species. Environ. Sci. Technol. 45, 514–519.
Phillips, J.C., Braun, R., Wang, W., Villa, E., Chipot, C., Skeel, R.D., et al., 2005. Scalable molecular dynamics with NAMD. J. Comput. Chem. 26, 1781–1802.
Pillar-Little, E.A., Camm, R.C., Guzman, M.I., 2014. Catechol oxidation by ozone and hydroxyl radicals at the air-water interface. Environ. Sci. Technol. 48, 14352–14360.
Renard, P., Siekmann, F., Gandolfo, A., Socorro, J., Salque, G., Ravier, S., et al., 2013. Radical mechanisms of methyl vinyl ketone oligomerization through aqueous phase OH-oxidation: on the paradoxical role of dissolved molecular oxygen. Atoms. Chem. Phys. 13, 6473–6491.
Ruiz-Lopez, M.F., Francisco, J.S., Martins-Costa, M.T., Anglada, J.M., 2020. Molecular reactions at aqueous interfaces. Nat. Rev. Chem. 4, 459–475.
Shi, Q., Zhang, W., Ji, Y., Wang, J., Qin, D., Chen, J., et al., 2020a. Enhanced uptake of glyoxal at the acidic nanoparticle interface: implications for secondary organic aerosol formation. Environ. Sci. Nano 7, 1126–1135.
Shi, Q., Zhang, W., Ji, Y., Wang, J., Qin, D., Chen, J., et al., 2020b. Enhanced uptake of glyoxal at the acidic nanoparticle interface: implications for secondary organic aerosol formation. Environ. Sci. Nano 7, 1126–1135.
Shouminng, Z., Ian, B., Tong, Z., Iustinian, B., Thorsten, B., 2008. Atmospheric chemistry of acetylacetone. Environ. Sci. Technol. 42, 7905–7910.
Song, W., Zhang, Y., Yu, J., Gao, Y., Naitoc, T., Oinumac, G., 2019. Rapid removal of polyacrylamide from wastewater by plasma in the gas-liquid interface. J. Environ. Sci. 83, 1–7.
Spencer, J.N., Holmboe, E.S., Kirshenbaum, M.R., Firth, D.W., Pinto, P.B., 1982. Solvent effects on the tautomeric equilibrium of 2,4-pentanedione. Can. J. Chem. 60, 1178–1182.
Tan, S., Zhang, X., Lian, Y., Chen, X., Yin, S., Du, L., et al., 2022a. OH group orientation leads to organosulfate formation at the liquid aerosol surface. J. Am. Chem. Soc. 144, 16953–16964.
Tan, S., Zhang, X., Lian, Y., Chen, X., Yin, S., Du, L., et al., 2022b. OH group orientation leads to organosulfate formation at the liquid aerosol surface. J. Am. Chem. Soc. 144, 16953–16964.
Teresa Baeza Romero, M., Blitz, M.A., Heard, D.E., Pilling, M.J., Price, B., Seakins, P.W., et al., 2005. Photolysis of methylethyl, diethyl and methylvinyl ketones and their role in the atmospheric HO_x budget. Farad. Discuss. 130, 73.
Torrie, G.M., Valleau, J.P., 1977. Nonphysical sampling distributions in Monte Carlo free-energy estimation: Umbrella sampling. J. Comput. Phys. 23, 187–199.
VandeVondele, J., Hutter, J., 2007. Gaussian basis sets for accurate

calculations on molecular systems in gas and condensed phases. J. Chem. Phys. 127, 114105.
VandeVondele, J., Krack, M., Mohamed, F., Parrinello, M., Chassaing, T., Hutter, J., 2005. Quickstep: fast and accurate density functional calculations using a mixed Gaussian and plane waves approach. Comput. Phys. Commun. 167, 103–128.
Verma, P.K., Koch, F., Steinbacher, A., Nuernberger, P., Brixner, T., 2014. Ultrafast UV-induced photoisomerization of intramolecularly H-Bonded symmetric β-diketones. J. Am. Chem. Soc. 136, 14981–14989.
Wang, X., Wei, Y., Zhang, H., Bao, L., He, M., Yuan, S., 2021. Understanding the properties of methyl vinyl ketone and methacrolein at the air-water interface: adsorption, heterogeneous reaction and environmental impact analysis. Chemosphere 283, 131183.
Wu, B., Zhang, G., Zhang, S., 2016. Fate and implication of acetylacetone in photochemical processes for water treatment. Water Res. 101, 233–240.
Xue, L., Gu, R., Wang, T., Wang, X., Saunders, S., Blake, D., et al., 2016. Oxidative capacity and radical chemistry in the polluted atmosphere of HongKong and Pearl River Delta region: analysis of a severe photochemical smogepisode. Atoms. Chem. Phys. 16, 9891–9903.
Yamabe, S., Tsuchida, N., Miyajima, K., 2004. Reaction paths of keto-enol tautomerization of β-diketones. J. Phys. Chem. A 108, 2750–2757.
Yao, L., Garmash, O., Bianchi, F., Zheng, J., Yan, C., Kontkanen, J., et al., 2018. Atmospheric new particle formation from sulfuric acid and amines in a Chinese megacity. Science 361, 278–281.
Zhang, F., Yu, X.F., Sui, X., Chen, J.M., Zhu, Z.H., Yu, X.Y., 2019. Evolution of aqSOA from the air-liquid interfacial photochemistry of glyoxal and hydroxyl radicals. Environ. Sci. Technol. 53, 10236–10245.
Zhang, T., Wen, M., Ding, C., Zhang, Y., Ma, X., Wang, Z., et al., 2023. Multiple evaluations of atmospheric behavior between Criegee intermediates and HCHO: Gas-phase and air-water interface reaction. J. Environ. Sci. 127, 308–319.
Zhang, W., Zhong, J., Shi, Q., Gao, L., Ji, Y., Li, G., et al., 2021. Mechanism for rapid conversion of amines to ammonium salts at the air-particle interface. J. Am. Chem. Soc. 143, 1171–1178.
Zhao, Y., Truhlar, D.G., 2008. The M06 suite of density functionals for main group thermochemistry, thermochemical kinetics, noncovalent interactions, excited states, and transition elements: two new functionals and systematic testing of four M06-class functionals and 12 other functionals. Theor. Chem. Acc. 120, 215–241.
Zhong, J., Kumar, M., Francisco, J.S., Zeng, X., 2018. Insight into chemistry on cloud/aerosol water surfaces. Acc. Chem. Res. 51, 1229.
Zhong, J., Li, H., Kumar, M., Liu, J., Liu, L., Zhang, X., 2019. New mechanistic insight into the reaction of organic acids with SO_3 at the air-water interface. Angew. Chem. Int. Ed. 58, 8351–8355.
Zhong, J., Zhao, Y., Li, L., Li, H., Francisco, J.S., Zeng, X., 2015. Interaction of the NH_2 radical with the surface of a water droplet. J. Am. Chem. Soc. 137, 12070–12078.
Zhong, J., Zhu, C., Li, L., Richmond, G.L., Francisco, J.S., Zeng, X.C., 2017. Interaction of SO_2 with the surface of water nanodroplet. J. Am. Chem. Soc. 139, 17168–17174.